ACS OMEGA

http://pubs.acs.org/journal/acsodf

Article

Quenching the Macroporous Collapse of Polyelectrolyte Multilayer Films for Repeated Drug Loading

Zi-Xuan Liang,[#] Qing-Shuang Li,[#] Zheng-Kun Zhao, Da Zhang, and Xia-Chao Chen*

Cite This: *ACS Omega* 2022, 7, 13853−13860

Read Online

ACCESS | Metrics & More | Article Recommendations | Supporting Information

ABSTRACT: Macroporous structures can be developed within polyelectrolyte multilayer films for efficient drug loading, but these structures tend to collapse or fracture during conventional drying procedures. Herein, a facile dehydrating method for macroporous polyelectrolyte multilayer films is proposed using solvent exchange to ethanol and then spontaneous evaporation. During these processes, the collapse of the macroporous structures can be effectively avoided, which can be ascribed to a combined effect of two factors. On one hand, capillary pressure during ethanol evaporation is relatively small since the surface tension of ethanol is much lower than that of water. On the other hand, solvent exchange suppresses the interdiffusion of polyelectrolytes and substantially increases the mechanical strength of the macroporous films, more than three orders of magnitude, making the pore walls highly tolerant of the capillary pressure. The stability of macroporous polyelectrolyte films to ethanol enables the repeated wicking from the ethanol solution of drugs, leading to a higher loading beyond previous studies. Such a high loading is favorable for the long-term release of drugs from the surfaces of modified substrates and maintaining a local drug concentration above the minimum effective concentration.

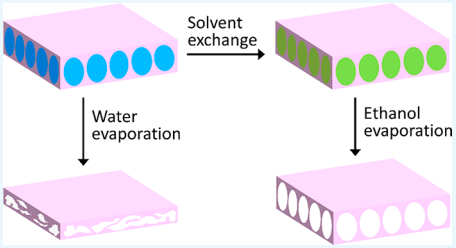

INTRODUCTION

There are a wide range of applications for porous polymeric films, including but not limited to drug delivery, separation, detection, and optics.[1−5] Layer-by-layer (LbL) assembly, based on the cyclical deposition of interacting species onto substrates, has emerged as a versatile tool to construct polymeric films with tunable thicknesses and compositions.[6,7] Taking advantage of the sensitivity of assembled units to external stimuli (electric field, pH, ionic strength, light, etc.), the internals of LbL-based polymeric films can be readily adjusted to generate various porous structures.[8−10] The formation of these porous structures are mainly determined by the composition of the LbL films, the type of interchain interactions (e.g., electrostatic, hydrogen-bonding, host−guest), and especially the interdiffusion of polymeric chains, which has been primarily investigated to understand the buildup mechanism of LbL films.[11] In general, porous structures on the nanometer scale are typically developed in LbL films with a limited level of chain interdiffusion.[12] In contrast, exponentially growing LbL films, which feature a high interdiffusion of polyelectrolytes throughout the whole films, can be exploited to fabricate macroporous films with a high porosity.[13−15] Using such macroporous platforms, we previously enabled the unprecedented loading of drugs by simply wicking from drug solutions, thus dramatically increasing the efficiency and reducing the complexities compared to other LbL films.[16] Other applications, such as super-hydrophobic surfaces,[17] ionic conductors,[18] and supports for catalysts,[19] can be also developed. Nevertheless, after formation in aqueous phases, the macroporous structures of exponentially growing LbL films tends to collapse or fracture during conventional drying procedures.[20] This is mainly caused by the impact of capillary pressures (P) on the pore walls and the low strength of the films related to the high mobility of polyelectrolytes.[21,22] Dehydrating by lyophilization[23,24] or supercritical carbon dioxide[25] can be an effective approach to retain these macroporous structures, but it involves the investment of specialized instrumentations and the problems associated with complicated operations. Therefore, a simple but efficient method is still desirable to dehydrate the macroporous LbL films before further applications.

In this study, we demonstrate that the interdiffusion of polyelectrolytes in LbL films can be restrained by exchanging water with ethanol. A facile dehydrating method for macroporous LbL films was applied using solvent exchange to ethanol and then spontaneous evaporation. During these processes, the collapse of the macroporous structures was found to be effectively avoided, which can be attributed to a combined effect of two factors. On one hand, quenching the interdiffusion of polyelectrolytes by solvent exchange substantially increases the mechanical strength of the macroporous films more than three orders of magnitude, making the pore

Received: January 10, 2022
Accepted: March 9, 2022
Published: April 12, 2022

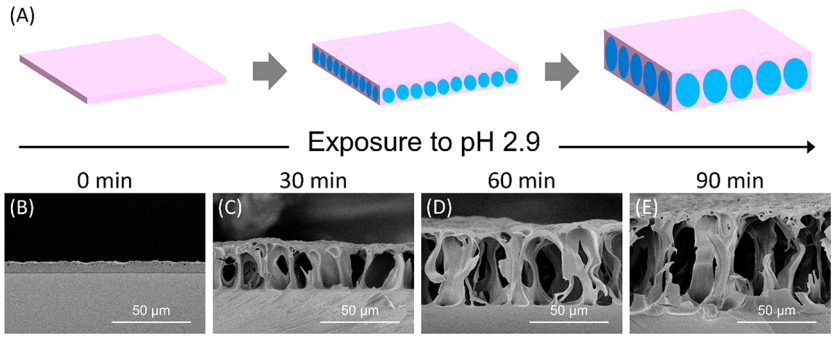

Figure 1. (A) $(PEI/PAA)_{15}$ films were immersed into an acidic solution (pH 2.9) to induce the formation of macroporous structures. (B–E) SEM cross-sectional images of $(PEI/PAA)_{15}$ films after being exposed to pH 2.9 for 0, 30, 60, and 90 min, respectively. Note that lyophilization was applied to dehydrate the samples before SEM observation.

walls highly tolerant of the capillary pressure. On the other hand, the capillary pressure ($P \approx \gamma$) during ethanol evaporation is relatively small since the surface tension of ethanol (γ = 22.9 mN m^{-1}) is much lower than that of water (γ = 71.6 mN m^{-1}). Compared to the other drying methods, this approach has the merits of simplicity, versatility, and low cost, and eliminates the investment of expensive and specialized instrumentations. Interestingly, the stability of macroporous LbL films to ethanol enabled their repeated wicking from the ethanol solution of drugs, leading to a higher loading beyond previous studies. Such a high loading is favorable for the long-term release of drugs from the surfaces of modified substrates and maintaining the local drug concentration above what is called the minimum effective concentration. Besides that, this study also provides unique insight into the chain mobility of LbL films, which correlates with the dynamic features of these films and may lead to their new applications as intelligent materials.

MATERIALS AND METHODS

Materials. Poly(ethylenimine) (PEI, M_w 25 000), poly(acrylic acid) (PAA, M_w 100 000), and a special cleaning concentrate (Hellmanex III) for glass substrates were purchased from Sigma-Aldrich (Germany). Triclosan, malachite green chloride, and fluorescein isothiocyanate isomer I (FITC) were obtained from Aladdin (Shanghai, China). Phosphate buffered saline (PBS) was purchased from Sangon Biotech (Shanghai, China). Hydrochloric acid (HCl) and sodium hydroxide (NaOH) were purchased from Beijing Chemical Works (China). Deionized water was produced through a water purification system (Millipore, America). The pH values of various aqueous solutions were adjusted by utilizing 1.0 M HCl or 1.0 M NaOH as needed. FITC-labeled PEI (PEI^{FITC}) was synthesized by mixing 5 mg of FITC into 80 mL of 0.5 wt % PEI aqueous solution and then maintaining the mixture at 4 °C for 48 h. After that, the mixture was dialyzed against deionized water for two weeks, and the final solution was freeze-dried to give an orange slime.

Film Assembly. Glass substrates were soaked in an aqueous solution (1.5 vol %) of Hellmanex III at 75 °C for 15 min and then rinsed with deionized water thoroughly. PEI/PAA films were constructed by alternately dipping the precleaned glass substrates into PEI solution (1 mg mL^{-1}, pH 9.0) for 15 min and PAA solution (3 mg mL^{-1}, pH 2.9) for 15 min. After each dipping step, the substrates were rinsed using deionized water and blown dry by a stream of nitrogen. These steps were repeated until a desired number of PEI/PAA bilayers were assembled onto the substrates. In this study, PEI/PAA films are referred to as $(PEI/PAA)_n$, where n corresponds to the number of PEI/PAA bilayers.

Post-Assembly Treatment. The as-prepared PEI/PAA films were dipped into a bath of acidic solution (pH 2.9) for a predetermined time to induce the development of macroporous structures. After that, the macroporous films were soaked into ethanol for 30 min to allow solvent exchange. The films were then taken out and put into a vacuum chamber to remove the residual ethanol. In this study, the effectiveness of this drying method was compared to that of lyophilization. Therefore, a series of macroporous films were dehydrated through a lyophilizer (Lichen LC-10N-50A, China) as a control.

Drug Loading and Release. The macroporous films were partially dipped into an ethanol solution of triclosan to enable the wicking process. The films were taken out and put into a vacuum chamber to remove the ethanol. This loading process can be repeated to further increase the loading amount. To measure the loading amount, triclosan was first extracted using ethanol from the films and then analyzed using a UV–vis spectrophotometer (Shimadzu UV-2600, Japan). The triclosan-loaded films were immersed in PBS (pH 7.4, 37 °C) to investigate their release kinetics. The PBS was frequently replaced with a fresh one to ensure a constant release condition, and the solutions were analyzed using the UV–vis spectrophotometer.

Zone Inhibition Test. Zone inhibition testing was carried out using *Escherichia coli* (ATCC 8739). Drug-loaded films (5 mm × 5 mm) were placed onto nutrient agar plates that had been seeded with 0.2 mL of bacterial suspension (1.0×10^7 CFU mL^{-1}). The plates were examined for a zone of inhibition after incubation at 37 °C overnight. An agar plate with a bare glass substrate (5 mm × 5 mm) was used as a control.

Characterization. The thickness of PEI/PAA films was measured using a thin-film analyzer (Filmetrics F20, America). Scanning electron microscopy (SEM, Hitachi S4800, Japan) was performed to reveal the structural features of samples as needed. The electrostatic interactions within polyelectrolyte multilayers were studied by attenuated total reflectance Fourier transform infrared spectroscopy (ATR-FTIR, Varian Excalibur 3100, America) in water, in ethanol, and in air. Note that the test in water was performed in D_2O instead of H_2O to reduce the overlap of the vibrational peaks of carboxylate band with a strong water band. The stiffness of PEI/PAA films was tested using a nanoindenter (Piuma Optics11, Netherlands) equipped with a 44.6 N probe. Fluorescence recovery after photobleaching (FRAP) experiments was investigated using a

https://doi.org/10.1021/acsomega.2c00204
ACS Omega 2022, 7, 13853–13860

confocal laser scanning microscope (Zeiss LSM800 with Airyscan, Germany) to demonstrate the interdiffusion of polyelectrolytes qualitatively. Briefly, a $(PEI^{FITC}/PAA)_{15}$ film was photobleached over a 20 μm circular region with a laser beam, and fluorescent images were subsequently captured at 0 and 15 min, respectively.

RESULTS AND DISCUSSION

There are two growth modes identified in the literature for polyelectrolyte multilayers, which can grow either linearly or exponentially depending on the mobility of polyelectrolytes "in" and "out" of the assemblies.[26,27] In this study, cationic poly(ethylenimine) (PEI) was LbL assembled with anionic poly(acrylic acid) (PAA) to yield an exponentially growing film. Both of these two species are weak polyelectrolytes with a low density of charges along main chains as well as sparse bonding sites to the assemblies, and their high mobility throughout the films has been well demonstrated by our own and others' previous studies.[28,29] After assembly, the PEI/PAA films was immersed in a bath of acidic solution (pH 2.9) to induce the formation of macroporous structures (Figure 1A). Such acid-induced transformation can be ascribed to the protonation of PEI ($pK_a \approx 6.5$) and PAA ($pK_a \approx 4.5-5.5$), dissociation of interchain ionic bonds, interdiffusion of polyelectrolyte chains, and subsequent phase separation.[30] Note that the PEI/PAA films can lose some polyelectrolytes during acid treatment, which has been systematically studied previously.[31] It has been found that the percentage of mass loss mainly depends on the pH value of acidic solutions and the duration of acid treatment. In our study, the percentage of mass loss is approximately 6.74% for a $(PEI/PAA)_{15}$ film exposed to pH 2.9 for 60 min, which was calculated by measuring the change of film mass before and after acid treatment (Figure S1).

In order to facilitate the characterization of morphological features, the films were further dehydrated by lyophilization to prevent the collapse of macroporous structures, which has been found to be inevitable during conventional dehydrating by evaporation. Figure 1B–E shows the cross-sectional images of $(PEI/PAA)_{15}$ films that had been exposed to pH 2.9 for different lengths of time. The pristine $(PEI/PAA)_{15}$ film appears compact and featureless, while a series of macroporous structures can be developed by acid treatment. The pore sizes were calculated to be 22.6 ± 3.5, 39.7 ± 5.4, and 52.9 ± 6.1 μm for macroporous $(PEI/PAA)_{15}$ films exposed to pH 2.9 for 30, 60, and 90 min, respectively. Extending the time of acid treatment also increased the thickness of the macroporous films as well as the volume of pore spaces. The porosity (v%) of the films was estimated using an equation described in our previous study:[16]

$$v\% = \frac{T_t - T_0}{T_t} \times 100\%$$

where T_t and T_0 are film thickness before and after acid treatment for a certain length of time (t), respectively. The film thickness was extracted from the SEM cross-sectional images of corresponding samples. The porosity of the films reached ~78.2% after 30 min of acid treatment, to ~84.5% after 60 min, and to ~90.1% after 90 min, respectively. In light of the positive correspondence between the macroporous structures and the length of time, applying acid treatment can be viewed as a reliable approach to tailor the porous structures within polyelectrolyte multilayers.

Although dehydrating by lyophilization is an effective approach to retain these macroporous structures,[16,32,33] it involves the investment of specialized instrumentations and the complexity associated with multistep operations. Therefore, a simple but efficient method is highly desirable to dehydrate macroporous polyelectrolyte films before further applications. In this study, a facile dehydrating method for the macroporous $(PEI/PAA)_{15}$ films was developed using solvent exchange to ethanol and then spontaneous evaporation (Figure 2A). Unlike

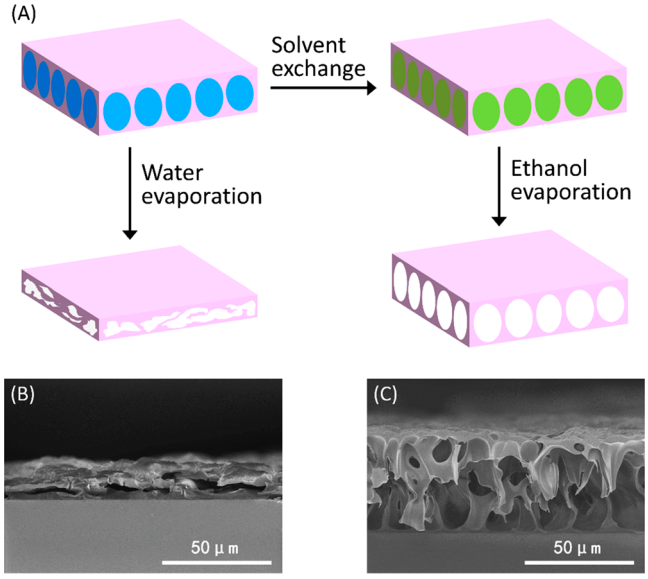

Figure 2. (A) Schematic of two dehydrating methods for macroporous polyelectrolyte films. One is to evaporate water directly, and the other involves solvent exchange to ethanol. The latter was followed by ethanol evaporation, which can be carried out without significantly affecting the profiles of the macroporous films. (B–C) SEM cross-sectional images of macroporous $(PEI/PAA)_{15}$ films exposed to pH 2.9 for 60 min and subsequently dehydrated using (B) direct water evaporation and (C) first solvent exchange to ethanol and then spontaneous evaporation.

direct water evaporation which led to the severe destruction of macroporous structures (Figure 2B), this dehydrating method made much less of an impact on the profiles of the macroporous films (Figure 2C). The performance of this method depends on the time of acid treatment as well as the characteristics of macroporous structures. For the macroporous films undergoing 30 and 60 min of acid treatment, this dehydrating method can effectively avoid the collapse of the macroporous structures (Figure S2), which is comparable to the effectiveness of lyophilization. Further prolonging the acid treatment will influence its applicability, resulting in a dehydrated film with slightly twisted pore walls (Figure S2). For example, after 90 min of acid treatment, macroporous films dehydrated by this method have a porosity of ~86.2%, slightly less than that of the same films dehydrated by lyophilization. It can be ascribed to the thinning of pore walls (Figure S2) and the lowering of their mechanical resistance against the capillary pressure of ethanol. Even so, this method can still be an attractive alternative to lyophilization considering its simplicity and cost advantage.

https://doi.org/10.1021/acsomega.2c00204
ACS Omega 2022, 7, 13853−13860

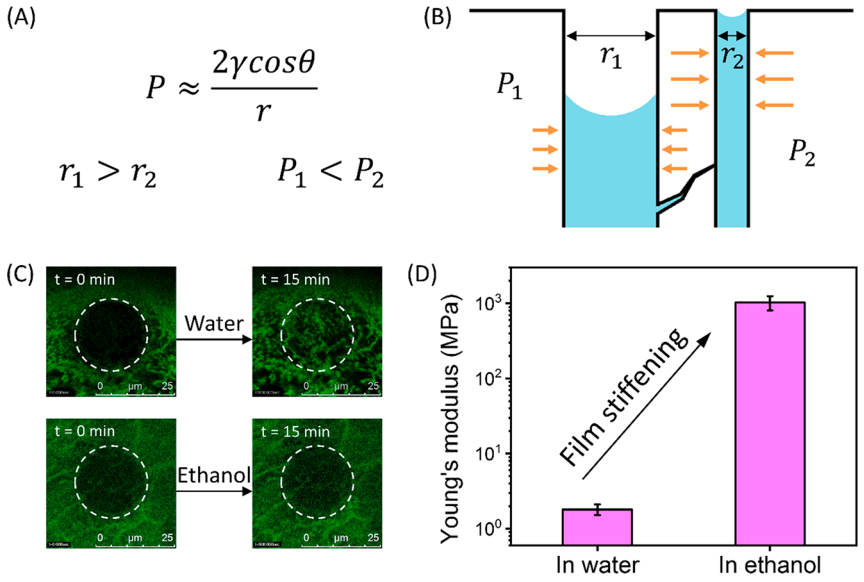

Figure 3. (A) An approximate equation describing that the magnitude of capillary pressure is related to the diameter (r) of pores, the surface tension (γ) of the contained liquid, and the contact angle (θ) between the liquid and the pore wall. (B) Schematic illustration of how a pore wall is collapsed by the impact of capillary pressures. Since the size of two neighboring pores is usually different, the capillary pressures on both sides of a pore wall are asymmetrical, and this produces a lateral force to collapse the porous structures. (C) Confocal microscope images of $(PEI^{FITC}/PAA)_{15}$ films taken at 0 and 15 min after photobleaching over a 20 μm circular region, which is marked using a dotted circle. The top set of images correspond to a sample immersed in deionized water, while the bottom set are that in ethanol. (D) Young's modulus of $(PEI/PAA)_{15}$ films in deionized water and in ethanol. It can be found that solvent exchange to ethanol substantially increases the mechanical strength of the films.

The structural collapse of macroporous films during traditional drying procedures, e.g., direct water evaporation, has been previously investigated in detail.[20] In this drying method, the vaporization of water forms liquid−vapor menisci within the porous structures, which recede over time and generate a capillary pressure (P) onto the pore walls.[34] The magnitude of such capillary pressure is related to the diameter (r) of pores, the surface tension (γ) of contained liquid, and the contact angle (θ) between the liquid and the pore wall,[21,35] as illustrated in Figure 3A. Since the size of two neighboring pores is usually different, the capillary pressures on both sides of a pore wall are asymmetrical, and this produces a lateral force to collapse the porous structures (Figure 3B). As an alternative, the macroporous $(PEI/PAA)_{15}$ films in this study was dehydrated using solvent exchange to ethanol and then spontaneous evaporation. Compared with water, which has a γ value as high as 71.6 mN m^{-1}, the surface tension of ethanol is much smaller, only 22.9 mN m^{-1}.[36] Therefore, the capillary pressure arising during ethanol evaporation is relatively small, which is favorable for the preservation of macroporous structures.

Besides reducing capillary pressure, exchanging water with ethanol also influences the interdiffusion of polyelectrolytes within $(PEI/PAA)_{15}$ films, as revealed by the fluorescence recovery after photobleaching (FRAP) experiments (Figure 3C). In such experiments, the recovery of fluorescence intensity in the bleached zone is generally due to the interdiffusion of unbleached fluorescent polyelectrolytes from outside of the zone.[37,38] As shown in Figure 3C, the fluorescence recovery of $(PEI/PAA)_{15}$ films in ethanol is considerably less noticeable than that in deionized water, indicating that the interdiffusion of polyelectrolyte chains can be effectively suppressed by solvent exchange to ethanol. Since the macroscopic strength of a polymeric material can be affected by its chain mobility,[22,39,40] we further tested the mechanical properties of $(PEI/PAA)_{15}$ films in deionized water and in ethanol (Figure 3D). It can be found that the Young's modulus of the films is 1030.98 ± 78.45 MPa in ethanol, which is three orders of magnitude higher than 1.81 ± 0.59 MPa in deionized water. The increased strength in ethanol can make the pore walls of macroporous $(PEI/PAA)_{15}$ films highly tolerant to the capillary pressure during ethanol evaporation and hence is beneficial to the stability of macroporous structures. It should be noted that the pH of deionized water is approximately 5.5, in which the formation of macroporous structures cannot be induced. Lowering the pH value to 2.9 can highly activate the interdiffusion of polyelectrolytes and enable the porous transition, but this makes the mechanical analysis very difficult to realize. Despite this, it can be reasonably deduced that the mechanical strength of PEI/PAA films in pH 2.9 is smaller than that in pH 5.5, considering the negative correlation between the mechanical strength of polymers and the mobility of polymeric chains.

The softening of PEI/PAA films in water seems quite understandable since water is a potent plasticizer for hydrophilic polymers. However, the PEI/PAA films are additionally stabilized by electrostatic interaction between $-NH^{3+}$ groups on PEI and $-COO^-$ groups on PAA. Therefore, the effect of water on such electrostatic interactions is crucial to understand the softening of the PEI/PAA films. As a solvent with a high dielectric constant (78.4 F m^{-1}, 25 °C), water has been studied as a potent plasticizer for polyelectrolyte multilayer systems, capable of disrupting ionic bonds between chains and increasing the free volume for the movement of chain segments.[37,38] In contrast, ethanol has a much lower dielectric constant, 24.3 F m^{-1} at 25 °C. Therefore, exchanging water with ethanol can make the interchain ionic bonds more difficult to dissociate and thus increase the resistance of chain mobility. Nevertheless, such an explanation remains to be verified by experimental data.

https://doi.org/10.1021/acsomega.2c00204
ACS Omega 2022, 7, 13853−13860

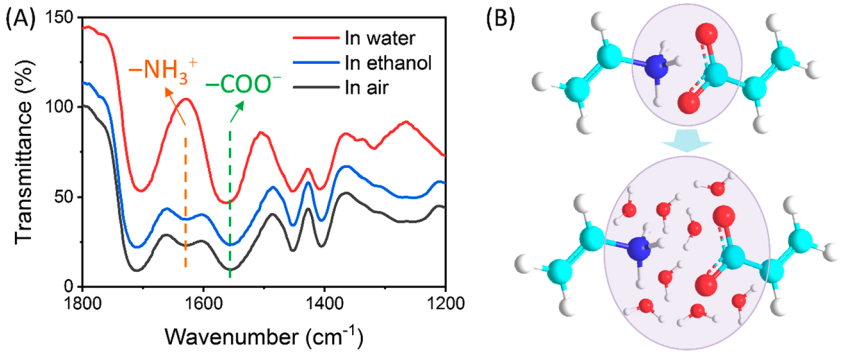

Figure 4. (A) ATR-FTIR spectra of a $(PEI/PAA)_{10}$ film tested in water, in ethanol, and in air. 1800−1200 cm^{-1} was chosen for analyzing the electrostatic interactions between $-NH^{3+}$ and $-COO^-$. 1627 cm^{-1} is assignable to the bending vibration of $-NH^{3+}$ groups, while 1554 cm^{-1} corresponds to asymmetric stretching vibration of $-COO^-$ groups. (B) Schematic illustration of how water molecules influence the electrostatic interactions between $-NH^{3+}$ and $-COO^-$. Note that vinylamine and acrylic acid were adopted here to represent PEI and PAA for the sake of simplicity.

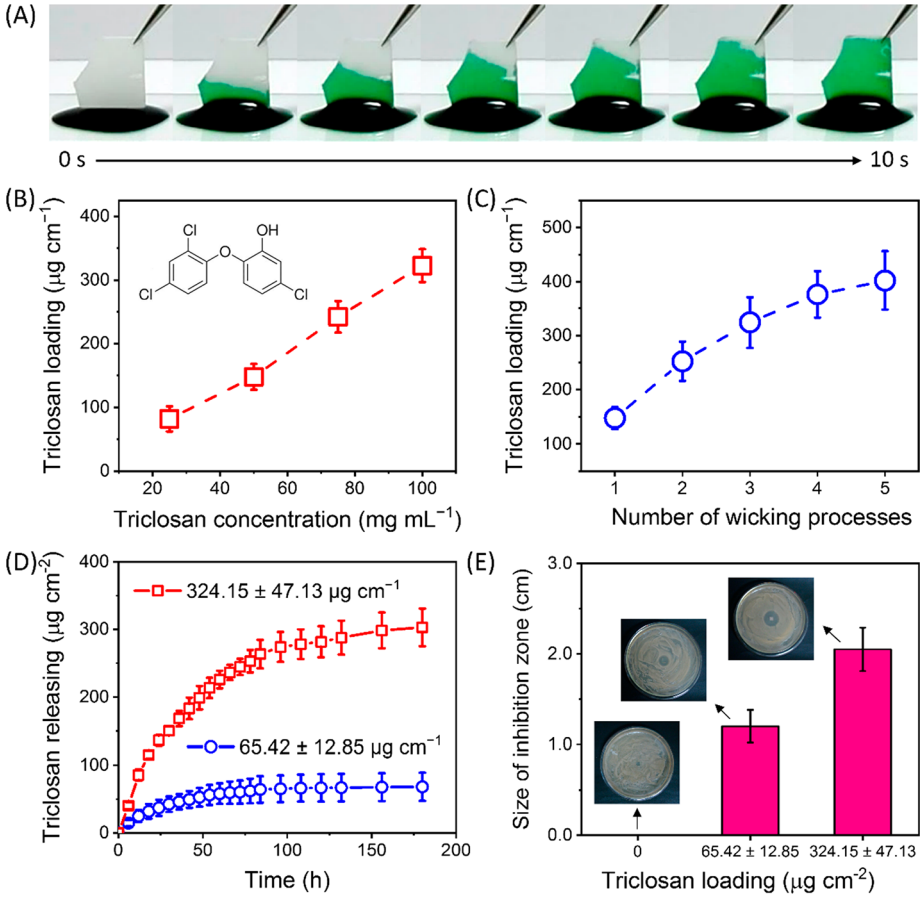

Figure 5. (A) Time-lapse images of a macroporous $(PEI/PAA)_{15}$ film wicking from an ethanol solution of malachite green (5 mg mL^{-1}), indicating the presence of an interconnected porous network across the whole film. (B) Plot of triclosan loading into a macroporous $(PEI/PAA)_{15}$ film with respect to the concentration of triclosan−ethanol solutions. The inset shows the molecular formula of triclosan. (C) Loading amount of triclosan into a macroporous $(PEI/PAA)_{15}$ film as a function of the number of its wicking from a triclosan−ethanol solution (50 mg mL^{-1}). (D) Release profiles of macroporous $(PEI/PAA)_{15}$ films with a triclosan loading of 65.42 ± 12.85 and 324.15 ± 47.13 $\mu g\ cm^{-1}$. (E) Inhibition zones against *Escherichia coli* of macroporous $(PEI/PAA)_{15}$ films with a triclosan loading of 0, 65.42 ± 12.85, and 324.15 ± 47.13 $\mu g\ cm^{-1}$, respectively. Insets are photographs of inhibition zones.

Accompanied by the screening of electrostatic interaction between PEI and PAA, the polarity of both the $-NH_3^+$ groups on PEI and the $-COO^-$ groups on PAA is expected to be attenuated. This can be verified through attenuated total reflectance Fourier transform infrared (ATR-FTIR) spectroscopy, which has been carried out in air, water, and ethanol, respectively. As shown in Figure 4A, 1800−1200 cm^{-1} was chosen for analyzing the electrostatic interactions between $-NH_3^+$ and $-COO^-$. 1627 cm^{-1} is assignable to the bending vibration of $-NH_3^+$ groups, while 1554 cm^{-1} corresponds to the asymmetric stretching vibration of $-COO^-$ groups. When the film was immersed in water from air, the vibrating peak of

https://doi.org/10.1021/acsomega.2c00204
ACS Omega 2022, 7, 13853−13860

$-NH_3^+$ groups entirely disappeared and that of $-COO^-$ groups shifted to a higher wavenumber. In contrast, these peaks remained almost unchanged in ethanol, indicating that water has a greater impact on the electrostatic interactions between $-NH_3^+$ and $-COO^-$ (Figure 4B).

In the past decade, the LbL technique has emerged as a striking tool for engineering drug delivery systems (DDSs) with controlled structure and composition.[41,42] Using macroporous $(PEI/PAA)_{15}$ films, we enabled the loading of drugs by simply wicking from their concentrated solutions,[43] thus dramatically increasing the efficiency and reducing the complexities compared to other LbL films. The wicking behavior of a macroporous $(PEI/PAA)_{15}$ film is illustrated in Figure 5A. When one end of the film came into contact with an ethanol solution of malachite green (a brilliant green dye for tracking liquid fronts), the green liquid rapidly climbed up the film, and only 10 s was spent to turn the whole film colored, implying the presence of an interconnected porous network across the whole film. Triclosan, a hydrophobic bactericide, was then used as a model drug to investigate the loading capacity of the films. As shown in Figure 5B, the loading amount of triclosan increases linearly with the concentration of triclosan−ethanol solutions, reaching 147.62 ± 20.25 $\mu g\ cm^{-1}$ for a given solution of 50 mg mL^{-1}. After the vaporizing of ethanol under a vacuum, the macroporous structures of the film can be well retained (Figure S3), and this facilitated another wicking from the drug solution. Actually, because of the stability of the macroporous films, the wicking process can be repeated multiple times, and drug loading can be increased correspondingly. Figure 5C shows that the loading amount of triclosan into a macroporous $(PEI/PAA)_{15}$ film with respect to the number of its wicking from a triclosan−ethanol solution (50 mg mL^{-1}). It can be found that the triclosan loading increased to an unprecedented value of 324.15 ± 47.13 $\mu g\ cm^{-1}$ after just three wicking processes. The drug loading can be further increased by increasing the wicking processes, although its increment will decline continuously (Figure 5C). The latter can be attributed to the occupation of pore volumes by the drug already loaded and the decrease of pore channels available for the next wicking process.

The release profile of triclosan from macroporous $(PEI/PAA)_{15}$ films was investigated by immersing the samples in PBS. As shown in Figure 5D, the duration of drug release can be increased with more drug loaded into the films. The releasing of triclosan lasted for ∼90 h when the films had a triclosan loading of 65.42 ± 12.85 $\mu g\ cm^{-1}$, while it dramatically increased to 180 h as the loading was up to 324.15 ± 47.13 $\mu g\ cm^{-1}$. Besides the releasing time, increasing drug loading can also affect the diffusion rate of a drug from the films. This can be qualitatively illustrated by an agar diffusion assay against *Escherichia coli*, given that triclosan is a bactericide. As demonstrated in Figure 5E, a film with a triclosan loading of 324.15 ± 47.13 $\mu g\ cm^{-1}$ formed a zone of inhibition larger than that with less triclosan loaded, indicating that more triclosan was released from the former within the same time. Increasing the diffusion rate of a drug from a substrate is favorable to maintain the local drug concentration above a certain level, which is essential to make the drug work effectively.[44−46]

CONCLUSIONS

In summary, a facile dehydrating method for macroporous polyelectrolyte multilayers was developed to avoid the collapse of macroporous structures. This approach was carried out simply using solvent exchange to ethanol and then spontaneous evaporation. Compared with conventional drying procedures, this method reduced the capillary pressure within the macropores and simultaneously increased the mechanical strength of the pore walls, both of which are favorable for the preservation of macroporous structures. Additionally, the stability of macroporous LbL films to ethanol facilitated their repeated wicking from the ethanol solution of drugs, leading to a higher loading beyond previous studies. Such a high loading is favorable for the long-term release of drugs from the surfaces of modified substrates and maintaining the local drug concentration above the minimum effective concentration.

ASSOCIATED CONTENT

Supporting Information

The Supporting Information is available free of charge at https://pubs.acs.org/doi/10.1021/acsomega.2c00204.

Change of film mass before and after acid treatment, SEM cross-sectional images of macroporous films dehydrated by the present method, and a macroporous film after wicking from an ethanol solution of triclosan and vaporizing ethanol under a vacuum (PDF)

AUTHOR INFORMATION

Corresponding Author

Xia-Chao Chen − *School of Materials Science & Engineering, Zhejiang Sci-Tech University, Hangzhou 310018, P. R. China*; orcid.org/0000-0002-8989-9336; Email: chenxiachao@zstu.edu.cn

Authors

Zi-Xuan Liang − *School of Materials Science & Engineering, Zhejiang Sci-Tech University, Hangzhou 310018, P. R. China*

Qing-Shuang Li − *School of Materials Science & Engineering, Zhejiang Sci-Tech University, Hangzhou 310018, P. R. China*

Zheng-Kun Zhao − *School of Materials Science & Engineering, Zhejiang Sci-Tech University, Hangzhou 310018, P. R. China*

Da Zhang − *School of Materials Science & Engineering, Zhejiang Sci-Tech University, Hangzhou 310018, P. R. China*

Complete contact information is available at: https://pubs.acs.org/10.1021/acsomega.2c00204

Author Contributions

#Z.-X.L. and Q.-S.L. contributed equally to this work.

Notes

The authors declare no competing financial interest.

ACKNOWLEDGMENTS

This research was supported by the financial support of the National Natural Science Foundation of China (Grant No. 22105174), the China Postdoctoral Science Foundation (Grant Nos. 2019M650435, 2021M691550), the Zhejiang Provincial Natural Science Foundation of China (Grant No. LQ21E030014), the Joint Funds of the Zhejiang Provincial Natural Science Foundation of China (Grant No. LZJWY22B070008), the Scientific Research Fund of the Zhejiang Provincial Education Department (Grant No.

Y202148238), and the Fundamental Research Funds of Zhejiang Sci-Tech University (Grant No. 2021Q011).

REFERENCES

(1) Mandal, J.; Fu, Y.; Overvig, A. C.; Jia, M.; Sun, K.; Shi, N. N.; Zhou, H.; Xiao, X.; Yu, N.; Yang, Y. Hierarchically Porous Polymer Coatings for Highly Efficient Passive Daytime Radiative Cooling. *Science* **2018**, *362*, 315−319.
(2) Park, H. B.; Kamcev, J.; Robeson, L. M.; Elimelech, M.; Freeman, B. D. Maximizing the Right Stuff: The Trade-Off between Membrane Permeability and Selectivity. *Science* **2017**, *356*, 356.
(3) Zhu, X.; Hao, J.; Bao, B.; Zhou, Y.; Zhang, H.; Pang, J.; Jiang, Z.; Jiang, L. Unique Ion Rectification in Hypersaline Environment: A High-Performance and Sustainable Power Generator System. *Sci. Adv.* **2018**, *4*, eaau1665.
(4) Wang, J.; Xue, Y.; Liu, J.; Hu, M.; Zhang, H.; Ren, K.; Wang, Y.; Ji, J. Hierarchical Capillary Coating to Biofunctionalize Drug-Eluting Stent for Improving Endothelium Regeneration. *Research* **2020**, *2020*, 1458090.
(5) Ding, Y.; Song, C.; Gong, W.; Liu, L.; Wu, M.; Li, L.; Yao, J. Robust, Sustainable, Hierarchical Multi-Porous Cellulose Beads Via Pre-Crosslinking Strategy for Efficient Dye Adsorption. *Cellulose* **2021**, *28*, 7227−7241.
(6) Borges, J.; Mano, J. F. Molecular Interactions Driving the Layer-by-Layer Assembly of Multilayers. *Chem. Rev.* **2014**, *114*, 8883−8942.
(7) Wagberg, L.; Erlandsson, J. The Use of Layer-by-Layer Self-Assembly and Nanocellulose to Prepare Advanced Functional Materials. *Adv. Mater.* **2021**, *33*, 2001474.
(8) An, Q.; Huang, T.; Shi, F. Covalent Layer-by-Layer Films: Chemistry, Design, and Multidisciplinary Applications. *Chem. Soc. Rev.* **2018**, *47*, 5061−5098.
(9) Monge, C.; Almodovar, J.; Boudou, T.; Picart, C. Spatio-Temporal Control of Lbl Films for Biomedical Applications: From 2d to 3d. *Adv. Healthcare Mater.* **2015**, *4*, 811−830.
(10) Yuan, W.; Weng, G. M.; Lipton, J.; Li, C. M.; Van Tassel, P. R.; Taylor, A. D. Weak Polyelectrolyte-Based Multilayers Via Layer-by-Layer Assembly: Approaches, Properties, and Applications. *Adv. Colloid Interface Sci.* **2020**, *282*, 102200.
(11) Volodkin, D.; von Klitzing, R. Competing Mechanisms in Polyelectrolyte Multilayer Formation and Swelling: Polycation−Polyanion Pairing Vs. Polyelectrolyte−Ion Pairing. *Curr. Opin. Colloid Interface Sci.* **2014**, *19*, 25−31.
(12) Hiller, J. A.; Mendelsohn, J. D.; Rubner, M. F. Reversibly Erasable Nanoporous Anti-Reflection Coatings from Polyelectrolyte Multilayers. *Nat. Mater.* **2002**, *1*, 59−63.
(13) Huang, W. P.; Chen, X. C.; Hu, M.; Wang, J.; Qian, H. L.; Hu, D. F.; Dong, R. L.; Xu, S. Y.; Ren, K. F.; Ji, J. Dynamic Porous Pattern through Controlling Noncovalent Interactions in Polyelectrolyte Film for Sequential and Regional Encapsulation. *ACS Appl. Mater. Interfaces* **2020**, *12*, 42081−42088.
(14) Chen, X.; Sun, J. Fabrication of Macroporous Films with Closed Honeycomb-Like Pores from Exponentially Growing Layer-by-Layer Assembled Polyelectrolyte Multilayers. *Chem. - Asian J.* **2014**, *9*, 2063−2067.
(15) Zhang, D.; Li, Q. S.; Liang, Z. X.; Chen, X. C.; Hao, J.; Yao, J.; Lu, C. X.; Zhou, Y.; Jiang, L. Laser-Directed Foaming of Hydroplastic Polyelectrolyte Films toward Tunable Structures and Programmable Routes. *Adv. Funct. Mater.* **2022**, *32*, 2107598.
(16) Chen, X.-C.; Ren, K.-F.; Zhang, J.-H.; Li, D.-D.; Zhao, E.; Zhao, Z. J.; Xu, Z.-K.; Ji, J. Humidity-Triggered Self-Healing of Microporous Polyelectrolyte Multilayer Coatings for Hydrophobic Drug Delivery. *Adv. Funct. Mater.* **2015**, *25*, 7470−7477.
(17) Yu, J.; Han, S.; Hong, J. S.; Sanyal, O.; Lee, I. Synchronous Generation of Nano- and Microscaled Hierarchical Porous Polyelectrolyte Multilayers for Superwettable Surfaces. *Langmuir* **2016**, *32*, 8494−8500.
(18) Zhang, W.; Zhao, Q.; Yuan, J. Porous Polyelectrolytes: The Interplay of Charge and Pores for New Functionalities. *Angew. Chem., Int. Ed.* **2018**, *57*, 6754−6773.
(19) Kanungo, S.; Paunovic, V.; Schouten, J. C.; Neira D'Angelo, M. F. Facile Synthesis of Catalytic Aupd Nanoparticles within Capillary Microreactors Using Polyelectrolyte Multilayers for the Direct Synthesis of H_2o_2. *Nano Lett.* **2017**, *17*, 6481−6486.
(20) Chen, X. C.; Ren, K. F.; Lei, W. X.; Zhang, J. H.; Martins, M. C.; Barbosa, M. A.; Ji, J. Self-Healing Spongy Coating for Drug "Cocktail" Delivery. *ACS Appl. Mater. Interfaces* **2016**, *8*, 4309−4313.
(21) Scherer, G. W.; Smith, D. M. Cavitation During Drying of a Gel. *J. Non-Cryst. Solids* **1995**, *189*, 197−211.
(22) An, N.; Wang, X.; Li, Y.; Zhang, L.; Lu, Z.; Sun, J. Healable and Mechanically Super-Strong Polymeric Composites Derived from Hydrogen-Bonded Polymeric Complexes. *Adv. Mater.* **2019**, *31*, e1904882.
(23) Cui, Y.; Wang, Y.; Shao, Z.; Mao, A.; Gao, W.; Bai, H. Smart Sponge for Fast Liquid Absorption and Thermal Responsive Self-Squeezing. *Adv. Mater.* **2020**, *32*, e1908249.
(24) Ali, I.; Hussain, R.; Louis, H.; Bokhari, S. W.; Iqabl, M. Z. In Situ Reduced Graphene-Based Aerogels Embedded with Gold Nanoparticles for Real-Time Humidity Sensing and Toxic Dyes Elimination. *Microchim. Acta* **2021**, *188*, 10.
(25) Padmajan Sasikala, S.; Poulin, P.; Aymonier, C. Prospects of Supercritical Fluids in Realizing Graphene-Based Functional Materials. *Adv. Mater.* **2016**, *28*, 2663−2691.
(26) Picart, C.; Mutterer, J.; Richert, L.; Luo, Y.; Prestwich, G. D.; Schaaf, P.; Voegel, J. C.; Lavalle, P. Molecular Basis for the Explanation of the Exponential Growth of Polyelectrolyte Multilayers. *Proc. Natl. Acad. Sci. U. S. A.* **2002**, *99*, 12531−12535.
(27) Gilbert, J. B.; Rubner, M. F.; Cohen, R. E. Depth-Profiling X-Ray Photoelectron Spectroscopy (Xps) Analysis of Interlayer Diffusion in Polyelectrolyte Multilayers. *Proc. Natl. Acad. Sci. U. S. A.* **2013**, *110*, 6651−6656.
(28) Chen, X. C.; Ren, K. F.; Chen, J. Y.; Wang, J.; Zhang, H.; Ji, J. Self-Wrinkling Polyelectrolyte Multilayers: Construction, Smoothing and the Underlying Mechanism. *Phys. Chem. Chem. Phys.* **2016**, *18*, 31168−31174.
(29) Wang, X.; Liu, F.; Zheng, X.; Sun, J. Water-Enabled Self-Healing of Polyelectrolyte Multilayer Coatings. *Angew. Chem., Int. Ed.* **2011**, *50*, 11378−11381.
(30) Chen, X. C.; Huang, W. P.; Hu, M.; Ren, K. F.; Ji, J. Controlling Structural Transformation of Polyelectrolyte Films for Spatially Encapsulating Functional Species. *Small* **2019**, *15*, e1804867.
(31) Cho, C.; Zacharia, N. S. Film Stability During Postassembly Morphological Changes in Polyelectrolyte Multilayers Due to Acid and Base Exposure. *Langmuir* **2012**, *28*, 841−848.
(32) Yu, Y.; Shi, X.; Liu, L.; Yao, J. Highly Compressible and Durable Superhydrophobic Cellulose Aerogels for Oil/Water Emulsion Separation with High Flux. *J. Mater. Sci.* **2021**, *56*, 2763−2776.
(33) Feng, S.; Deng, J.; Yu, L.; Dong, Y.; Zhu, Y.; Fu, Y. Development of Lightweight Polypyrrole/Cellulose Aerogel Composite with Adjustable Dielectric Properties for Controllable Microwave Absorption Performance. *Cellulose* **2020**, *27*, 10213−10224.
(34) García-González, C. A.; Camino-Rey, M. C.; Alnaief, M.; Zetzl, C.; Smirnova, I. Supercritical Drying of Aerogels Using Co2: Effect of Extraction Time on the End Material Textural Properties. *J. Supercrit. Fluids* **2012**, *66*, 297−306.
(35) Li, C.; Dai, H.; Gao, C.; Wang, T.; Dong, Z.; Jiang, L. Bioinspired Inner Microstructured Tube Controlled Capillary Rise. *Proc. Natl. Acad. Sci. U. S. A.* **2019**, *116*, 12704−12709.
(36) Wang, L.; Zhao, Y.; Tian, Y.; Jiang, L. A General Strategy for the Separation of Immiscible Organic Liquids by Manipulating the Surface Tensions of Nanofibrous Membranes. *Angew. Chem., Int. Ed.* **2015**, *54*, 14732−14737.
(37) Wang, J.; Xue, Y. F.; Chen, X. C.; Hu, M.; Ren, K. F.; Ji, J. Humidity-Triggered Relaxation of Polyelectrolyte Complexes as a Robust Approach to Generate Extracellular Matrix Biomimetic Films. *Adv. Healthcare Mater.* **2020**, *9*, e2000381.
(38) Krebs, T.; Tan, H. L.; Andersson, G.; Morgner, H.; Gregory Van Patten, P. Increased Layer Interdiffusion in Polyelectrolyte Films

https://doi.org/10.1021/acsomega.2c00204
ACS Omega 2022, 7, 13853−13860

Upon Annealing in Water and Aqueous Salt Solutions. *Phys. Chem. Chem. Phys.* **2006**, *8*, 5462−5468.
(39) Chen, X. C.; Sun, P.; Sun, T.; Yu, Z.; Chen, F.; Chen, Y.; Liu, H. Ionically Conductive Pastes as Conformable Collector for Transparent, Nonplanar Triboelectric Devices. *Adv. Electron. Mater.* **2020**, *6*, 1900668.
(40) Wang, F.; Li, Z.; Guo, J.; Liu, L.; Fu, H.; Yao, J.; Krucińska, I.; Draczyński, Z. Highly Strong, Tough, and Stretchable Conductive Hydrogels Based on Silk Sericin-Mediated Multiple Physical Interactions for Flexible Sensors. *ACS Appl. Polym. Mater.* **2022**, *4*, 618−626.
(41) Costa, R. R.; Mano, J. F. Polyelectrolyte Multilayered Assemblies in Biomedical Technologies. *Chem. Soc. Rev.* **2014**, *43*, 3453−3479.
(42) Ren, K.-f.; Hu, M.; Zhang, H.; Li, B.-c.; Lei, W.-x.; Chen, J.-y.; Chang, H.; Wang, L.-m.; Ji, J. Layer-by-Layer Assembly as a Robust Method to Construct Extracellular Matrix Mimic Surfaces to Modulate Cell Behavior. *Prog. Polym. Sci.* **2019**, *92*, 1−34.
(43) Lei, W.-x.; Chen, X.-c.; Hu, M.; Chang, H.; Xu, H.; Ren, K.-f.; Ji, J. Dynamic Spongy Films to Immobilize Hydrophobic Antimicrobial Peptides for Self-Healing Bactericidal Coating. *J. Mater. Chem. B* **2016**, *4*, 6358−6365.
(44) Park, K. Controlled Drug Delivery Systems: Past Forward and Future Back. *J. Controlled Release* **2014**, *190*, 3−8.
(45) Zhang, Y.; Zhao, R.; Liu, J.; Kong, H.; Zhang, K.; Zhang, Y. N.; Kong, X.; Zhang, Q.; Zhao, Y. Hierarchical Nano-to-Molecular Disassembly of Boron Dipyrromethene Nanoparticles for Enhanced Tumor Penetration and Activatable Photodynamic Therapy. *Biomaterials* **2021**, *275*, 120945.
(46) Ruan, L.; Song, G.; Zhang, X.; Liu, T.; Sun, Y.; Zhu, J.; Zeng, Z.; Jiang, G. Transdermal Delivery of Multifunctional Cao2@Mn-Pda Nanoformulations by Microneedles for Nir-Induced Synergistic Therapy against Skin Melanoma. *Biomater. Sci.* **2021**, *9*, 6830−6841.

https://doi.org/10.1021/acsomega.2c00204
ACS Omega 2022, 7, 13853−13860